remote sensing

MDPI

Article

Evaluation of the ABI/GOES-16 SST Product in the Tropical and Southwestern Atlantic Ocean

Mayna Helena Azevedo, Natália Rudorff * and José Antônio Aravéquia

Instituto Nacional de Pesquisas Espaciais, Dutra km 39, Cachoeira Paulista 12227-010, São Paulo, Brazil; mayna.azevedo@inpe.br (M.H.A.); jose.aravequia@inpe.br (J.A.A.)

* Correspondence: natalia.rudorff@inpe.br; Tel.: +55-12-3208-7687

Abstract: Sea surface temperature (SST) is an essential climate variable used for ocean and weather monitoring and forecasting. The NOAA's next generation geostationary satellite GOES-16 was declared operational at the east position (75°W) in December 2017, carrying onboard an Advanced Baseline Imager (ABI). The hyperspectral ABI sensor now allows SST estimates every 10–15 min at both day and nighttime, with advanced options for cloud screening and water vapor correction. In the present work, we compare the first operational ABI SST product (OSI SAF, 2018) with an in situ match-up database (MDB) across the Tropical and Southwestern Atlantic Ocean, off the Brazilian coast, throughout the year of 2018. The MDB was obtained from two long-term programs, i.e., PIRATA moored buoys (FOLTZ et al., 2016) and PNBoia moored and drifting buoys (MARINHA DO BRASIL, 2017). Separate comparisons were made for each data set, analyzing the uncertainties according to the program (i.e., buoy type and region), satellite SST quality level and influence of diurnal heating. We also compare the ABI product with the OSTIA analysis L4 SST (DONLON et al., 2012) to increment our analyses on the spatio-temporal biases within the study region. The results show that the OSI SAF ABI SST L3C has a mean bias (0.1 °C) and error (RMSE, 0.5 °C) within the GHRSST standards, with an exception being coastal waters off the southeast Brazilian coast (RMSE, 0.65 °C), which are subjected to sharp thermal fronts. The highest biases are for regions/seasons subjected to persistent cloud coverage and high water-vapor content, i.e., the Intertropical and South Atlantic Convergence Zones, as well as highly dynamic frontal zones, i.e., the Brazil Malvinas Confluence Zone, the Subtropical Front and coastal waters. The ABI SST product is suitable for operational use, and applications should explore more deeply the new set of information provided.

Keywords: SST; ABI/GOES-16; South Atlantic Ocean

Citation: Azevedo, M.H.; Rudorff, N.; Aravéquia, J.A. Evaluation of the ABI/GOES-16 SST Product in the Tropical and Southwestern Atlantic Ocean. *Remote Sens.* **2021**, *13*, 192. https://doi.org/10.3390/rs13020192

Received: 19 November 2020
Accepted: 29 December 2020
Published: 8 January 2021

1. Introduction

The sea surface temperature (SST) is an important regulator of several ocean–atmosphere interaction processes, such as the exchange of heat, water, gas and momentum between the atmosphere and the ocean [1]. SST influences not only the ocean–atmosphere interface, but also higher levels of the boundary layer and even the troposphere, being an important essential climate variable (ECV) [2]. Precise and accurate SST measurements, both in long time series and in Near Real Time (NRT) products are thus essential for environmental studies and the operational monitoring and forecast of the ocean, weather and climate [2,3]. With the evolution of orbital remote sensing, radiometric instruments onboard geostationary and polar satellites have become essential to monitor and collect information from areas that are not covered by in situ data collection programs, especially in the open ocean [4] and in the Southern Hemisphere.

SST satellite products are generated from the brightness temperature (BT) measured by thermal infrared or microwave sensors, at atmospheric window channels (with minimum atmospheric gas absorption), and converted into SST by means of algorithms that combine external sources of information, using radiative transfer equations [5,6], empirical

regression analysis [7–9] or even machine learning techniques [10]. Such algorithms, in general, offer accurate SST estimates in global analyses [2,11]. At the regional and local levels, however, there are a number of factors that can generate higher uncertainties, such as greater effects of the absorption of water vapor and aerosols [12,13]. On a global scale, the desired accuracy for SST is a maximum bias of 0.5 °C in time scales of less than one day and resolution of at least 10 km [11]. At the regional and local levels, the required accuracy is even higher (0.2 °C) [14] to ensure the accurate detection of mesoscale and submesoscale processes [3].

One of the newest SST products released for operational use is from the NOAA's next generation Geostationary Operational Environmental Satellites, GOES-16, launched in 2016, and declared operational at the East position (75°W) in December 2017, covering the American continent and the adjacent eastern Pacific and western Atlantic oceans. The GOES-16's mission is to provide timely, high-quality, relevant information for meteo-oceanographic monitoring over the Americas and adjacent oceans. The hyperspectral Advanced Baseline Imager (ABI) onboard GOES-16 provides Full Disk imaging every 10–15 min in 16 channels from the visible to thermal infrared spectral region at 0.5- to 2-km resolution. This sensor allows the determination of SST for each cloud-free pixel over water during the entire diurnal cycle, with advanced options for cloud screening and water vapor correction [12,15,16]. The previous Imager (on board GOES-13, and others) only allowed nighttime SST estimates with limited accuracy. Such new information of the diurnal cycle and high resolution spatio-temporal processes should bring about advances in the monitoring and study of meteorological and oceanographic phenomena, especially in highly dynamic regions [3]. In the South Atlantic, some processes that may gain insights from such information are the role of sharp thermal fronts modulating the boundary layer, especially within the Brazil-Malvinas Confluence Zone (BMC) [17] and coastal upwelling cells [18], development of maritime-coastal fogs, marine thunderstorms, sea breezes and lines of instability, among others. The operational use in data assimilation systems is also expected to improve ocean-weather forecasts in the region. This, however, demands high-quality data products which should be evaluated and characterized in terms of levels and sources of uncertainty before use.

At the same time, the ABI/GOES-16 SST product provides higher temporal resolution information compared to other products, e.g., from polar-orbiting satellites; however, it may also have higher levels of uncertainty, which is inherent to geostationary satellite sensors. There are currently two operational ABI SST products under the GHRSST standards, i.e., one from the NOAA Center for Satellite Applications and Research (STAR) group and another from the EUMETSAT Sea Ice Satellite Applications Facility (OSI SAF) group. The OSI SAF ABI SST (L3) [16] was the first to be declared operational, whereas the NOAA STAR product underwent a couple of updates and reformulations before operational release [12,15].

The purpose of this work is to characterize the uncertainties of the ABI/GOES-16 SST product by comparing it with standard SST measurements and products over the Tropical and Southwestern Atlantic Ocean. The ABI/GOES-16 SST OSI SAF L3C product, hereafter referred to as SSTsat, was chosen for this study as it was the first to be declared operational. The SSTsat was compared to an in situ match-up database (MDB) collected over the study region throughout an entire yearly cycle (2018). The MDB was obtained from fixed and drifting buoys of two long-term programs: the Prediction and Research Moored Array in the Tropical Atlantic (PIRATA) [19] and the National Buoy Program (*Programa Nacional de Boias*, PNBoia) [20]. A comparison was also made with a standard SST analysis L4 product, i.e., OSTIA, to identify regions and/or periods with greater uncertainty across the entire Tropical and Southwestern Atlantic Ocean. The NOAA Geo-Polar Blended SST analysis product was also used for comparison, but since the results were very similar to those from the OSTIA comparison, the latter was selected to show the results for this study.

Study Region

The study region was defined to cover the Tropical and Southwestern Atlantic from 65°W to 20°W and 10°N to 45°S. The spatio-temporal variability of the SST in the study region was relatively high, varying from approximately 5–15 °C (monthly average) in the Southern most sector (>35°S) during the austral winter (July–August), to 25–35 °C (monthly average) in the Tropical Atlantic (10°S–10°N) (Figure 1).

Some meteorological and oceanographic features and processes that are important for this study region, with potential impacts on the SST satellite retrievals, are indicated in Figure 1. There are two atmospheric convergence zones that form persistent cloudy bands, i.e., the Intertropical Convergence Zone (ITCZ) and the South Atlantic Convergence Zone (SACZ) [21]. The ITCZ is formed by the convergence of trade winds and has a southward displacement during the austral summer (December–February) (~1°N) and northward shift during the austral winter (June–August) (~8°N) [22]. The SACZ occurs generally in the austral summer and is related to several conditions including the northward displacement of the South Atlantic Subtropical High, that allows cloudy and rainy conditions to actuate over Southeast Brazil. The cloudy band of the SACZ usually extends from the southern Amazon to central-eastern Brazil, and the adjacent South Atlantic Ocean, and lasts for at least five days [23].

In terms of the hydrography, the study region encompasses the Brazilian western boundary current, which is a poleward current that transports warm tropical waters near the Brazilian shelf break, and encounters the northward Falklands/Malvinas Current (MC), which transports cold Subantarctic waters, at the Brazil-Malvinas Confluence Zone (BMC) [24,25]. The southernmost sector of the study region is also characterized by the South Atlantic Subtropical Front (STF) which forms the boundary between subtropical and subpolar waters [26]. The BMC and the STF are both highly dynamic regions with sharp thermal fronts, and have an equatorward displacement during the austral winter and poleward shift during the austral summer, varying from ~30–45°S (Figure 1B) (note that the study region encompasses only part of the STF).

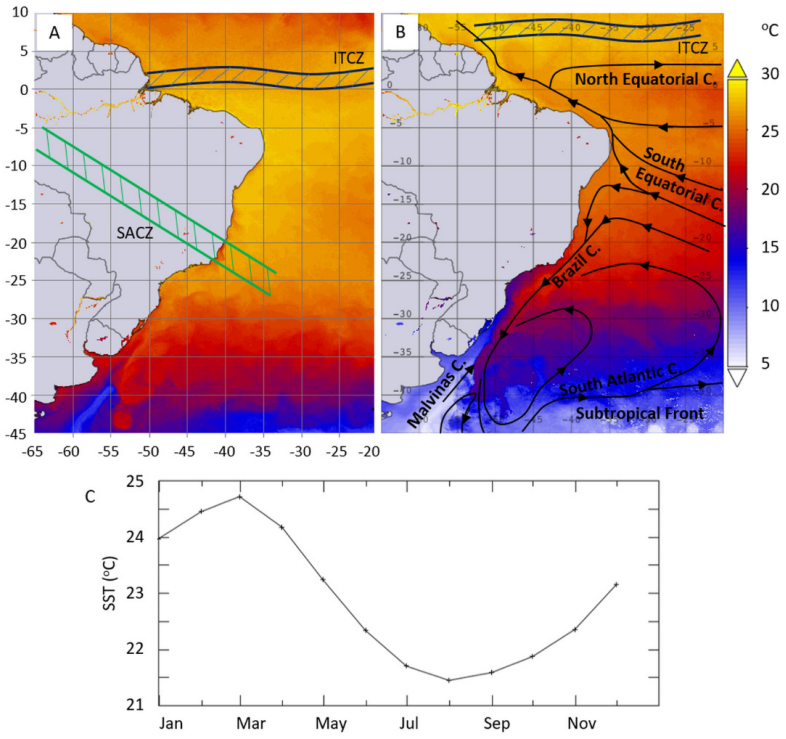

Figure 1. Monthly means MODIS-Aqua SST of March (**A**) and August (**B**) 2018, indicating the mean position of the ITCZ [22] and SACZ [23], and oceanic currents and fronts (adapted from [26]); and the average SST for the entire study region throughout 2018 (**C**).

2. Data

2.1. Match-up Data Base (MDB)

The moored buoys of the PIRATA program are located at the Tropical Atlantic, whereas the PNBoia program has coastal moored buoys off the Brazilian coast and drifting buoys across the Southern Atlantic. For both programs, only the buoys within the study region were selected, making, in total, seven PIRATA buoys, four PNBoia moored buoys and several drifting buoys (Figure 2).

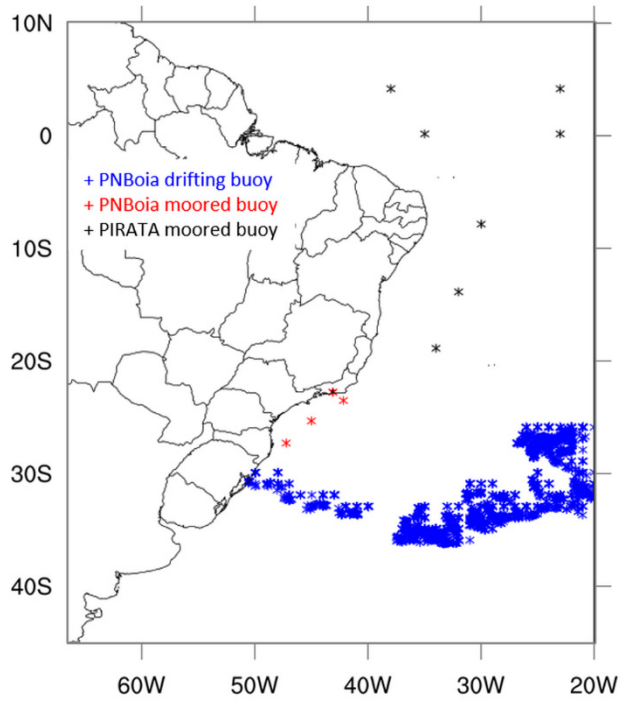

Figure 2. Study region indicating the location of the moored and drifting buoys used for the match-up data base.

2.1.1. PIRATA Project

The PIRATA project is an observation system founded in the mid-1990s for the Tropical Atlantic Ocean, composed mainly of moored buoys [19]. The project is a partnership between Brazil, France and the United States, with the purpose of studying the ocean–atmosphere interactions in the Tropical Atlantic that affect climatic variability. The data are collected and stored at 10-minute intervals, with public availability for daily averages transmitted to the Argos satellite system and distributed through GTS. The in situ SST (SSTdepth) is measured at 10 depth levels from 1 m to 500 m. For our purposes, daily averages collected at 1 m were selected. Auxiliary data of wind speed are also available and were used to compare the SST data without (>6 m.s^{-1}) influence of diurnal heating [27].

2.1.2. PNBoia Project

As a complement to the PIRATA project, Brazil implemented a network of meteorological buoys to contribute to Brazil's Global Ocean Observing System (GOOS-BRASIL; www.goosbrasil.org), including the *Programa Nacional de Boias* (PNBoia) [20]. The program started in December 1999, providing meteorological and oceanographic data in the Tropical and Southwest Atlantic Ocean, remedying the lack of data in the region (which is still limited), with 21 moored buoys (ATLAS) on the coast and 297 drifting buoys deposited in the South Atlantic (many of which have already been disabled). For the present study, we were able to obtain data only from four moored buoys located near the southeastern Brazilian coast, as well as from the drifting buoys in the Southern Atlantic (Figure 2). The data has public availability for hourly averages, but is collected randomly (not temporally

continuous). For the moored buoys, SSTdepth is collected at 1 m, and for the drifting buoys, at 0.2 m. Wind speed was not available in this case, so the data set was separated in terms of "all conditions" and "only nighttime" to analyze the influence of diurnal heating.

2.2. Satellite SST

2.2.1. ABI GOES-16 SST

The ABI sensor, onboard GOES-16 (GOES-East, at 75°W) has a field of view centered at the Eastern region of the Americas, covering from 60°N to 60°S, and 135°W to 15°W. This hyperspectral sensor performs Full Disk imaging every 10–15 min (depending on the scanning mode), which allows the composition of images every hour for the generation of SST L2 and L3 gridded products, with 2-km resolution at nadir and 12-km resolution at high satellite view zenith angles (~67°) [15].

The GHRSST Level 3C subskin SST GOES-16 ABI (GDS V2), produced by the Ocean and Sea Ice Satellite Application Facility (OSI SAF), is an hourly average product projected on a regular grid with a 0.05° resolution. The SST is determined within a complex processing chain at every pixel that passes through the nowcasting (NWC) cloud mask [28], and is identified as clear sky over the ocean. The "noncorrected" SST is then derived using a split window nonlinear regression algorithm (NL) [7] with three spectral window channels centered at 8.5, 10.3 and 12.3 µm [16,29,30] (Equation (1)).

$$SST = (a + bS_\theta)T_{8.5} + (c + dT_{CLI} + eS_\theta)(T_{10.3} - T_{12.3}) + gS_\theta + f \quad (1)$$

a, b, c, d, f and g are the regression coefficients determined from BT simulations on a radiosonde profile database [31], with the offset coefficient corrected relative to buoy measurements. T_{CLI} is the climatological SST value. $S_\theta = \sec(\theta_{sat}) - 1$, where, θ_{sat} is the satellite zenith angle.

The 8.5-µm channel is used in conjunction with the 10.3- and 12.3-µm channels for the determination of both daytime and nighttime SST, as well as for improved detection of thin cirrus clouds and correction for atmospheric humidity [15,16].

An incremental algorithm is then used to reduce regional/seasonal biases by comparing observed and simulated BTs (using OSTIA L4 SST, NWF profiles and radiative transfer equations), averaged over the last 20 days to reduce the uncertainties in the simulated BTs [30].

Finally, a quality control (QC) was created to inform the quality level of SST estimates for each pixel, with increasing levels from 0 to 5, classified as: no data (0), invalid (1), not used (2), good (3), very good (4) and excellent (5). This information is provided together with the SST product for every pixel that does not contain cloud mask. Only quality levels 3 to 5 are recommended for use [16], and thus, were selected for use in this study.

2.2.2. OSTIA SST Analysis

The OSTIA L4 SST analysis was developed as a contribution by the UK Meteorological Institute (UK-Met-Office) to the international GHRSST effort to provide global SST products for NWF, ocean model assimilation, environmental analysis and monitoring of ocean–atmosphere systems [32]. SST analysis is produced on an operational daily basis at the UK-Met-Office using optimal interpolation (OI) in a global grid with 0.054° resolution. The sensors used to compose the final product are the Advanced Very High Resolution Radiometer (AVHRR/NOAA and MetOP), Spinning Enhanced Visible and Infrared Imager (SEVIRI/MSG), Advanced Baseline Imager (GOES-16), Infrared Atmospheric Sounding Interferometer (IASI/MetOP), a microwave imager and in situ data from ships and buoys. The sea-ice concentration is obtained from the EUMETSAT OSI-SAF product [33].

Quality control of the OSTIA data in order to obtain a better representation of the SST of the foundation depth (SSTfnd, ≈10 m, without influence of diurnal heating [27]) led to the rejection of some values. Observations when the sun was above the horizon (at daytime) and wind speed less than 6 m.s^{-1} were rejected, to prevent the inclusion of daytime measurements with thermal stratification between the SST depths: skin (10 µm),

subskin (1 mm) and foundation (10 m). Satellite SST data that measures SSTskin included in the analysis were adjusted to compensate for skin temperature bias for wind speed above 6 m.s^{-1}, adding 0.17 °C to the SST measurement [27]. The quality control also has an algorithm that checks the background in relation to the previous analysis SST, using a priori estimates of background errors and observation errors [32]. The optimal interpolation method used for OSTIA is the Analysis Correction Method [34,35].

3. Methods

This work is divided into two main parts: (i) the first is the comparison of the SSTsat (ABI-GOES-16) with the MDB (SSTdepth) obtained from moored and drifting buoys to verify the quality of the satellite product in the study region; and the second (ii) is the comparison of the daily average SSTsat (ABI-GOES-16) with the global SSTfnd analysis (OSTIA).

3.1. SSTsat (ABI) vs. SSTdepth (MDB)

The SSTsat was compared to the in situ MDB obtained from the PIRATA and PNBoia programs, within the study region (Figure 2), for the year of 2018. The comparisons with were made using hourly averages for the PNBoia data, and daily averages for the PIRATA data.

To identify the levels and sources of uncertainty, the MDB was divided into different sets according to the program, type of buoy (moored or drifting) and SST depth, without influence of diurnal heating (>6 m.s^{-1} of wind speed for PIRATA data, and only nighttime SST for PNBoia data), and according to the quality level (QL) of the SSTsat product (3–5). We also used two spatial matching strategies: one using only the centered pixel and another within a searching window of 5 × 5 pixel. For simplicity, we only show the results of the centered pixel MDB, since the comparisons were very similar. The main differences were that the centered pixel had a lower number of match-ups, but generally better statistics, especially for the sharp thermal gradient regions (BMC and STF).

Since the in situ data is also subjected to measurement uncertainties, we applied a quality control criterion in order to identify spurious errors and remove spurious SSTs from the analyses, using the Interquartile Range statistical method (IQR). The IQR method is an important indicator of the variability of the data, and was used to identify outliers.

The statistics used to characterize the uncertainties of SSTsat were the root mean squared error (RMSE) and determination coefficient (from linear regression analysis), standard deviation (SD), absolute difference (AD) and bias (mean deviation) to ascertain systematic and random errors.

3.2. SSTsat (ABI) vs. SSTfnd (OSTIA)

A comparison between SSTsat (ABI/GOES-16) and the analysis SSTfnd (OSTIA global product) was made within the study region (Figure 1) for the year of 2018, using the resampled daily average interpolated to match the same grid size (0.054°) of both products. The daily average SSTsat was obtained using only nighttime data and daytime with wind speed greater than or equal to 6 m.s^{-1} (for all pixels with QL between 3–5) to exclude diurnal heating influence. The wind speed was provided along with the ABI-GOES-16 product, obtained from a NWF [16]. For the spatial resampling, Bilinear Interpolation was used with the OSTIA product as reference. The results are expressed in terms of monthly average maps of the difference between SSTfnd (OSTIA)–SSTsat (ABI).

It is important to mention again that there are several high quality L4 SST analysis products under the GHRSST standards. The NOAA Geo-Polar Blended SST analysis product (Geo-Polar-Blended-OSPO-L4-GLOB-v1.0) was also tested for comparison, but since the results were very similar to those from the OSTIA comparison, the OSTIA product was selected to show the results for the sake of simplicity.

4. Results

4.1. SSTsat (ABI) vs. SSTdepth (MDB)

The comparisons of SSTsat with SSTdepth had an overall good agreement for the MDBs, with relatively low deviation (R^2 between 0.82 to 0.96) and bias (<0.06 °C) (Figure 3). The best performance was with the daily average SSTdepth of the PIRATA moored buoys with lowest RMSE (<0.4 °C) (Figure 3C,D), and SSTdepth varying from 24–29 °C. The comparison with the hourly SSTdepth of the PNBoia drifting buoys had higher RMSE (0.59 °C) but also a high determination coefficient (R^2, 0.96) and low bias (0.045 °C), and with SSTdepth representing a higher range: 14–29 °C. The comparison with the hourly SSTdepth of the PNBoia coastal moored buoys had the highest error statistics (RMSE, 0.65 °C), with an SSTdepth ranging from 18–30 °C.

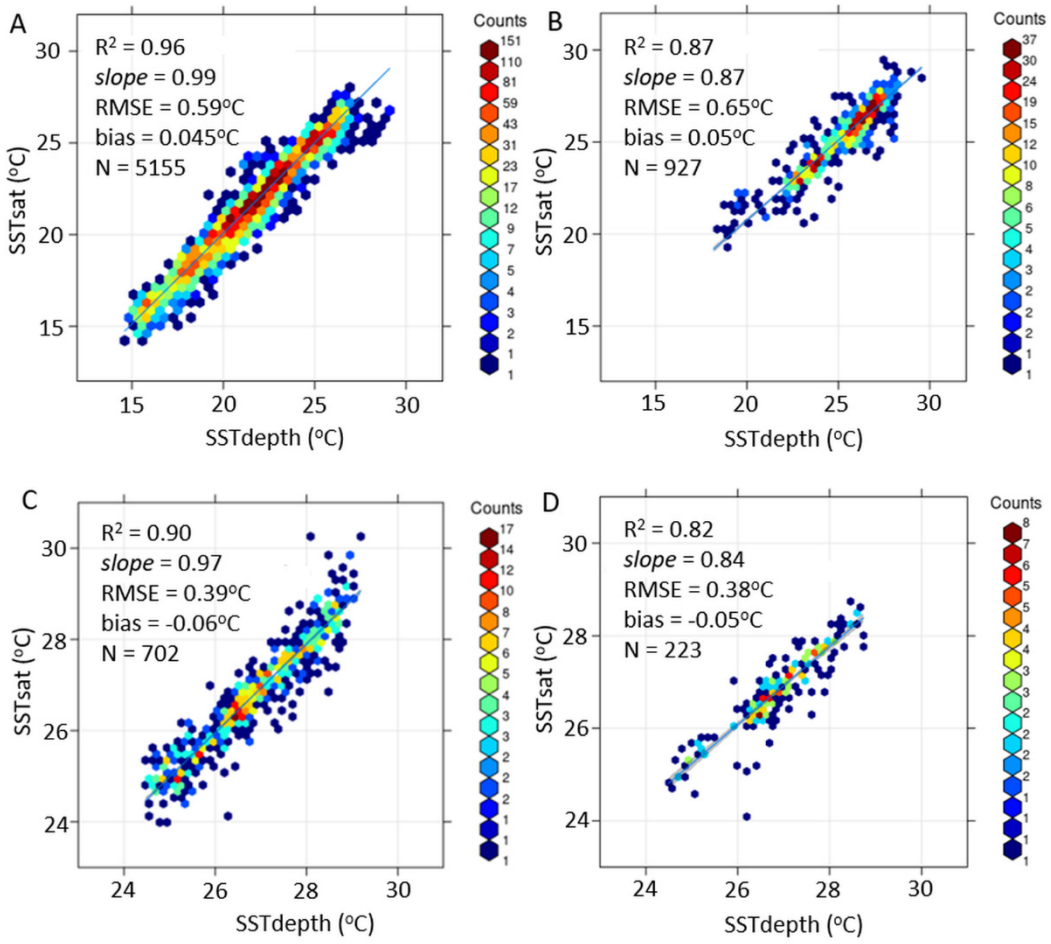

Figure 3. Scatterplots between SSTsat (ABI) (QL 3–5) and the in situ MDB of PNBoia drifting (**A**) and moored (**B**) buoys, and of the PIRATA moored buoys for all conditions (**C**) and for wind speed $\geq$ 6 m.s^{-1} (**D**). All graphs indicate the mean error statistics.

For the comparison of SSTsat with the PNBoia drifting buoys (SSTdepth at 0.2 m), there was an improvement in the statistics for higher QL (Table 1), but with a significant decrease in the number of match-ups, corroborating the recommendation to use the three best QLs to increase the coverage of retrieved SSTsat [16,36]. The higher absolute difference (0.4 °C) and RMSE (0.59 °C) obtained for the nighttime period could, however, also associated be with higher uncertainties in the cloud screening algorithm due to the lack of visible data [28,37].

Table 1. Statistics for the difference between SSTsat and SSTdepth of the PNBoia drifting buoys, separated by SSTsat quality level (QL) (3–5) and day and nighttime conditions, with the number of observations (N), root-mean-square error (RMSE, °C), bias (°C) and absolute difference (AD, °C).

	Night				Day			
QL	**N**	**RMSE**	**Bias**	**AD**	**N**	**RMSE**	**Bias**	**AD**
5	579	0.526	−0.040	0.403	729	0.477	0.062	0.365
4	943	0.618	0.043	0.446	1160	0.561	0.073	0.420
3	806	0.602	−0.008	0.450	938	0.546	0.121	0.426
3–5	2328	0.590	0.005	0.436	2827	0.536	0.086	0.408

For the comparisons of SSTsat with the PNBoia moored buoys (SSTdepth at 1m), along the Brazilian southeast coast, the errors and biases were relatively low for QL 5 (RMSE, 0.4 °C), but significantly higher for QL 3 and 4 (0.8–1 °C RMSE) (Table 2). A point to consider is the much lower number of match-ups obtained for these two cases (<134), which likely influenced the statistics. Highly dynamic coastal regions may also pose higher challenges for such match-up exercises between satellite and in situ SST [3]. Daytime bias was positive and nighttime negative, which was consistent with the comparisons with the drifting buoys.

Table 2. Statistics for the difference between SSTsat and SSTdepth of the PNBoia moored buoys, separated by SSTsat quality level (QL) (3–5), day and nighttime conditions, with the number of observations (N), root-mean-square error (RMSE, °C), bias (°C) and absolute difference (AD, °C).

	Night				Day			
QL	**N**	**RMSE**	**Bias**	**AD**	**N**	**RMSE**	**Bias**	**AD**
5	259	0.408	−0.013	0.290	344	0.441	0.094	0.308
4	81	0.817	−0.102	0.577	134	0.847	0.071	0.565
3	40	1.050	−0.123	0.737	69	1.149	0.344	0.851
3–5	380	0.612	−0.044	0.398	547	0.682	0.120	0.439

For the comparison of SSTsat with the daily average SSTdepth (1 m) of the moored buoys of the PIRATA project in the Tropical Atlantic, there was also an improvement in the statistics as the QL increased, but the errors and biases for QLs 3 and 4 in this case were still reasonably good (≤0.4 °C RMSE, <0.1 °C bias) (Table 3). When removing the match-ups under conditions of wind speeds lower than 6 m.s^{-1}, the error was slightly lower for SSTsat, even though the number of match-ups reduced significantly (e.g., 42 to 15 for QL 5) (Table 3). This highlights the importance of removing data which may have been significantly subjected to daytime thermal stratification when comparing SSTsat with in situ MDBs [27].

Table 3. Statistics of the difference between SSTsat and SSTdepth of the PIRATE moored buoys, separated by SSTsat quality level (QL) (3–5) for all conditions, and only for wind speed ≥ 6 m.s^{-1}, with the: number of observations (N), root-mean-square error (RMSE, °C), bias (°C) and absolute difference (AD, °C).

	SST1m (All Conditions)				SST1m (≥6 m.s^{-1})			
QL	**N**	**RMSE**	**Bias**	**AD**	**N**	**RMSE**	**Bias**	**AD**
5	42	0.226	−0.046	0.162	15	0.116	−0.027	0.092
4	259	0.328	−0.031	0.254	84	0.288	−0.010	0.227
3	401	0.437	−0.086	0.315	124	0.452	−0.087	0.310
3–5	702	0.390	−0.063	0.284	223	0.382	−0.054	0.264

All comparisons had a normal distribution of biases, with the majority of the differences being centered around zero. The histogram of the SST differences for the PNBoia

moored and drifting buoys were slightly skewed towards more positive biases, whereas the differences for the PIRATA moored buoys had more negative biases (Figure 4). Positive biases at higher latitudes (> 20°S) were also observed by [36] which compared the same ABI SST product (OSI SAF) to in situ MDBs across the Atlantic Ocean (for May 2018). No plausible explanation was devised by the authors in this case. In contrast, negative biases at the Tropical Atlantic were attributed to unmasked atmospheric aeolian dust bursts from the Sahara Desert [36].

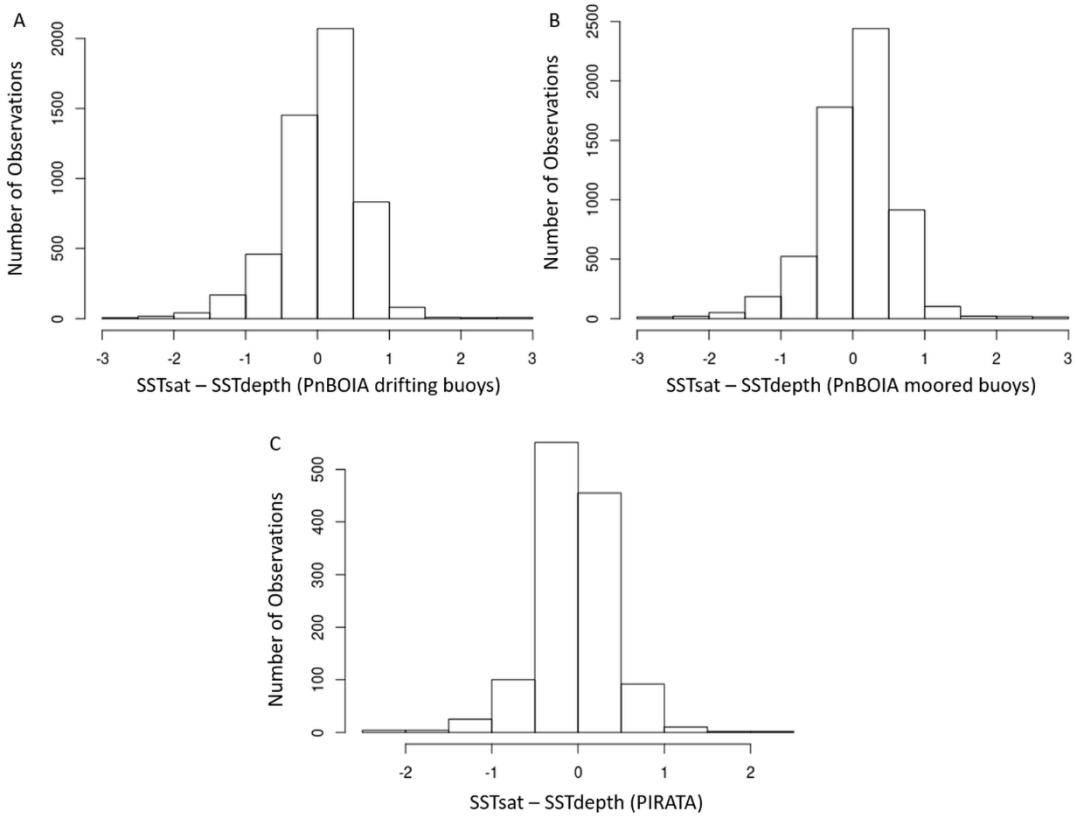

Figure 4. Histograms of the differences between SSTsat and the PNBoia drifting buoys (**A**), moored buoys (**B**) and PIRATA buoys (**C**).

The dependency of the SST differences on the geographical location (latitude and longitude), SST range and diurnal heating/cooling processes was analyzed in more detail for the PNBoia drifting buoys, as this MDB had hourly data, a reasonable number of observations (5155) and a higher range of SST values (Figures 5 and 6).

No strong dependencies were observed, but only some slight tendencies which could reveal the influence of some interferences. The positive biases for higher latitudes (> 20°S) were observed only up to 35°S. South of that the biases become negative (up to −39°S) (Figure 5A). This could be associated with higher effects of vapor absorption along the slant line of sight, which increases substantially at higher satellite zenith angles [12,36,38]. The differences in respect to the longitude profile, on the other hand, did not reveal any tendency (Figure 5B). For the SST values, there was only a slight increase in both positive and negative biases at the extremes, associated with a decrease in the number of observations (Figure 5C).

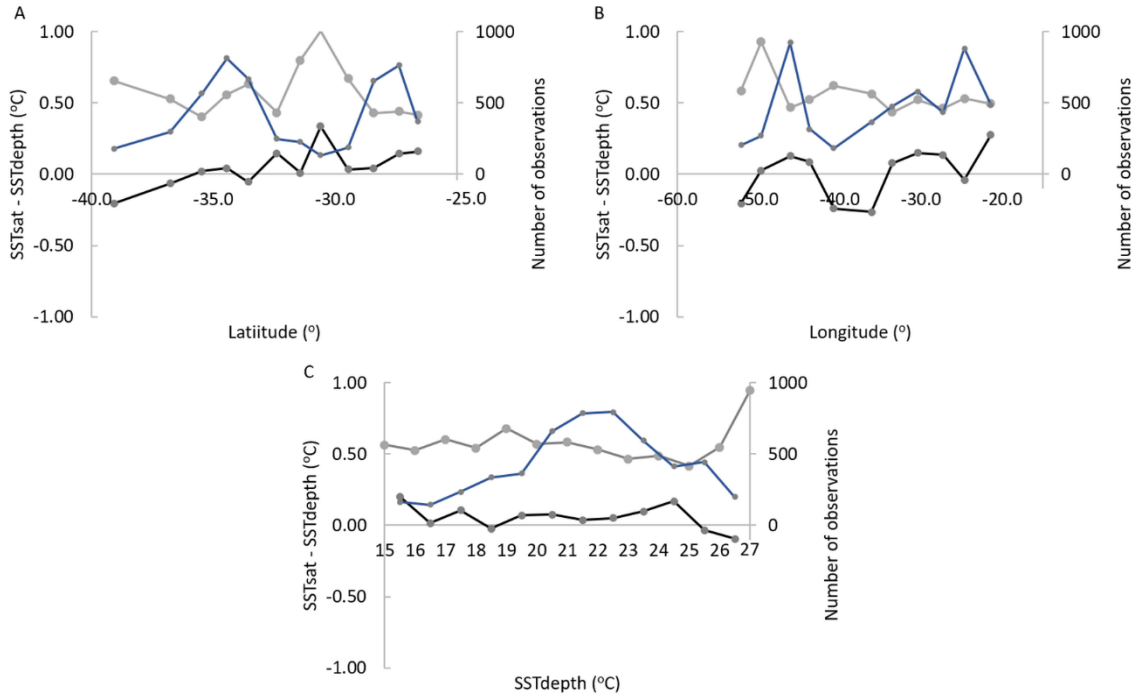

Figure 5. Difference between SSTsat and SSTdepth of the PNBoia drifting buoys vs. latitude (**A**), longitude (**B**) and SSTdepth (**C**). Mean bias is the black solid line, SD is the gray solid line and number of observations is the blue solid line.

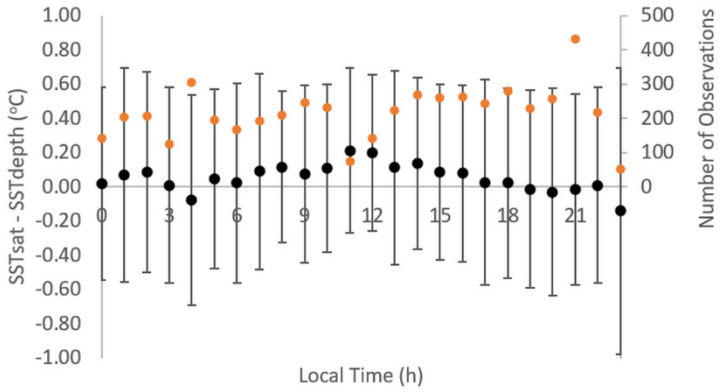

Figure 6. Hourly differences between SSTsat and SSTdepth (PNBoia drifting buoys) (diurnal mean deviation) (black points with the SD as error bars), and number of observations (orange points).

For the hourly differences between SSTsat and SSTdepth the highest positive values were obtained at the warmest daytime (11–12 h local time) with a mean difference of 0.20–0.21 °C, and the highest negative values at nighttime (maximum of −0.14 °C at 23 h) (Figure 6). These values however also coincided with a lower number of observations (50–140), and need to be viewed with caution. Nevertheless, one may note a higher frequency of positive biases during daytime (6–18 h) and negative during nighttime, revealing the higher influence of diurnal heating/cooling processes on SSTsat, as expected. The high SD values (0.44–0.84) also suggest high local differences.

4.2. SSTsat (ABI) vs. SSTfnd (OSTIA)

Regarding comparisons of the ABI GOES-16 SSTsat with the OSTIA analysis SSTfnd, the monthly mean differences were generally close to zero within most of the study region, especially for the central South Atlantic (0–30°S), with exceptions for some months and regions (Figure 7). January had the highest mean differences (up to 2 °C), with cooler SSTsat over most of the region. December showed a similar pattern but with lower differences.

Cooler ABI SSTsat can be partly explained by higher water vapor absorption and cloud contamination [39], which are typically higher in the South Atlantic during the austral summer months (December–February), especially within the ITZC and SACZ (Figure 1). For the other months, cooler ABI SSTsat values were more constrained in the Tropical Atlantic (10°N to 10°S) and/or the southernmost sector of the study region (south of 30°S). The Tropical Atlantic showed higher biases (1–2 °C), especially during the ITCZ southward displacement in the austral summer, and at the northernmost eastern sector, which is known to be influenced by aeolian dusts blown from the Sahara Desert, and transported by trade winds across the Atlantic [13].

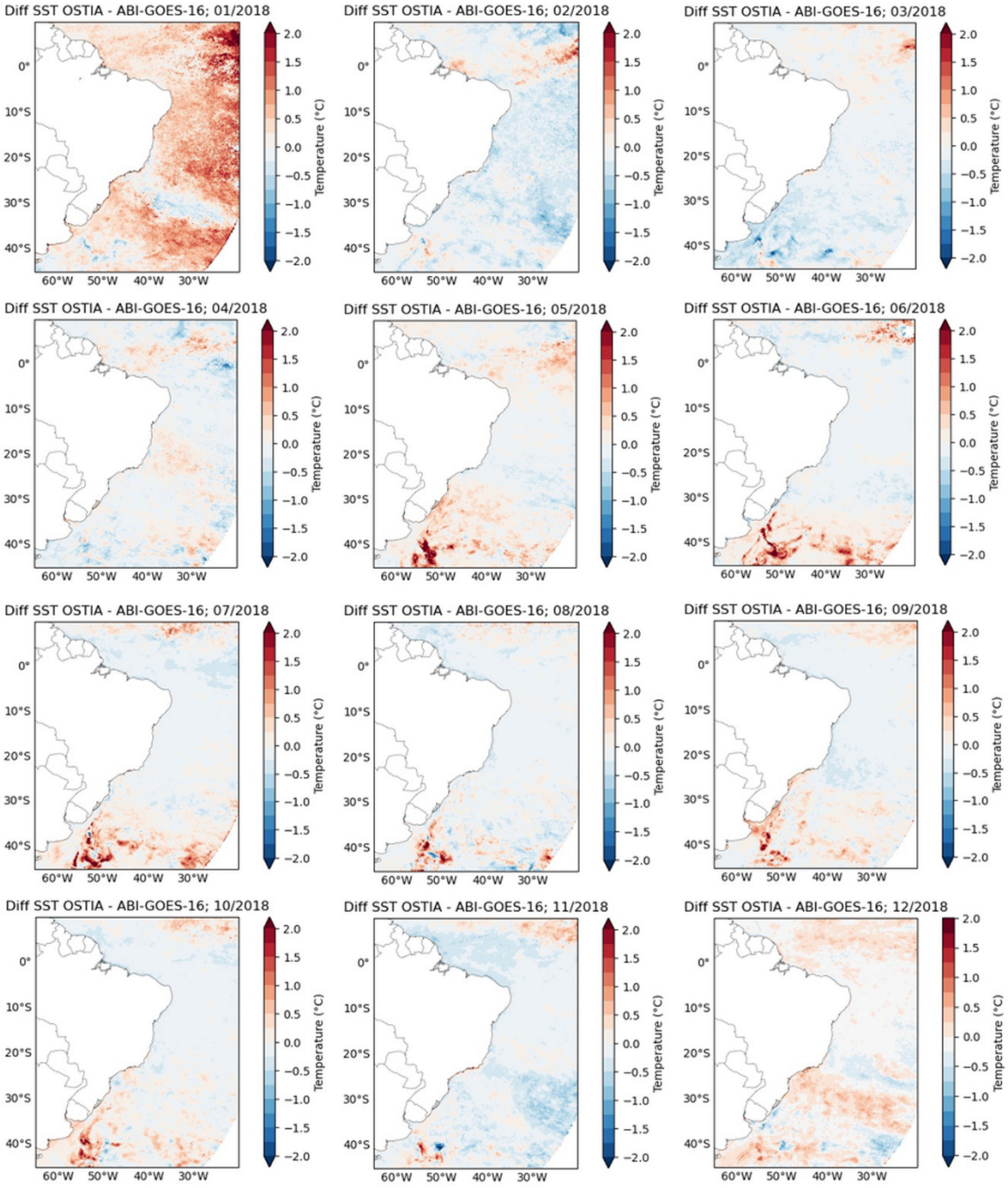

Figure 7. Monthly average difference maps of SSTfnd OSTIA – SSTsat ABI/GOES-16.

The Southern Atlantic (>30°S) showed a seasonal pattern of cooler ABI SST from May to October, and warmer ABI SST, especially from February to April. The highest differences (up to 2 °C) were observed at the BMC and STF (30–45°S), especially from May to November, when there is a northward displacement of these frontal zones (see Figure 1 for reference of their locations). Similar patterns of higher biases at the Tropical and Southern Atlantic have also been reported in other works analyzing the same ABI product [36] and other SST products as well [40].

5. Discussion

The comparisons of SSTsat with the in situ MDBs showed an overall good agreement, with a mean bias (<0.1 °C) and RMSE (~0.5 °C) within the GHRSST recommendations. The exception was only for the coastal moored buoys of the PNBoia program, for which SSTsat presented higher RMSE (0.65 °C).

The higher errors obtained for the moored coastal buoys may also reflect the increased difficulty of obtaining good match-ups at the coastal zone which, in this case, is subjected to sharp thermal fronts, such as at the Cape Frio upwelling cell off Rio de Janeiro (~23° S) [18]. Two of the four buoys analyzed were located within this cell. The other two buoys were near the shelf break and were also likely subjected to sharp thermal gradients, especially during the austral winter, when a northward coastal current transporting a mixture of Subantarctic waters and the La Plata river plume formed a coastal front with the warm tropical waters transported by the Brazilian Current [41]. The SSTdepth comprised a relatively high range of values (18–30 °C), indicating the presence of these coastal fronts. Deviations caused by subgrid scale (<0.05°) SST variability may be allowed. This, however, does not explain all the errors. Upwelling radiation from the adjacent continent is another source that may affect the SST satellite signal from coastal waters and increase match-up differences [42]. Regular maintenance and calibration of the sensors of the PNBoia moored buoys has also been reported to be challenging, posing higher uncertainties for in situ MDB [20].

The errors statistics for the Southern Atlantic (PNBoia drifting buoys) were also somewhat higher than for the Tropical Atlantic (PIRATA), likely due to the more challenging conditions for the SSTsat geostationary retrievals in the region, including higher satellite zenith angle, with higher atmospheric attenuation and lower spatial resolution [12], sharp thermal fronts (at the BMC and STF) and persistent cloud coverage, especially during the austral winter (with frequent passage of cold fronts). The hourly averaged SST values of both SSTsat and SSTdepth are also likely to have higher levels of uncertainty than daily averaged values, which were used for the PIRATA comparison.

Regarding the QLs of SSTsat, the results reinforce the recommendations of the OSI SAF validation report [36], i.e., to use QLs 3–5 to increase the number of observations without compromising significantly the quality of the retrieved SSTsat. An exception was the PNBoia coastal moored buoys, but the low number of observations may also have compromised the analysis.

The positive bias obtained for daytime and negative bias for nighttime match-ups denotes the higher influence of solar radiation heating during the daytime, and heat loss at night, on SSTsat compared to SSTdepth. Similar behavior was also observed by Picart and Marsouin (2018) for the same ABI SST product, as well as for other SST geostationary products in other works [12,43]. The differences between the temperature measured by thermal infrared radiometers, which correspond to the most superficial layer of skin (10 μm), and the temperature measured by in situ sensors from moored and drifting buoys (0.2−1 m), can reach up to 2 °C, depending on the thermal stratification [27]. The regression SST algorithm is adjusted to in situ SSTdepth with an offset correction [29,30], and the retrieved satellite SST is representative of SSTdepth, but is still sensitive to changes in the skin layer [12]. While this poses a challenge for satellite and in situ SST match-ups, it is a key advantage of geostationary SST observations, as the sensitivity of SSTsat to skin

and subskin SST variations provides information regarding the diurnal heating/cooling processes in a layer which is important for air–sea interactions [12,43].

With respect to the regional biases, the more negative biases in SSTsat observed for the Tropical Atlantic, both for the MDB comparison and the SSTfnd product, were likely related to the higher influence of water vapor absorption and subpixel cloud contamination at the ITCZ [39]. Influence of atmospheric aeolian dust from the Sahara Desert is also a major source of uncertainty in the northeastern Tropical Atlantic [13]. Dust absorbs the upwelling radiation and reemits at higher levels, thereby decreasing the radiance (and BT) measured at top of the atmosphere, leading to underestimations of the retrieved SSTsat. The OSI SAF ABI SST product has a correction term for Sahara dust, but it seems to be insufficient, as also observed in other works [36].

The positive biases at higher latitudes seemed to be either localized (20–35°S) or seasonal, as also shown with the SSTfnd comparison. Higher ABI SST errors in the region for were also observed in other works [12,36]. The Southern Atlantic (>20°S) is characterized by the presence of highly dynamic sharp thermal fronts, especially within the BMC and STF (30–45°S). The spatial pattern of the biases revealed by the SSTfnd comparison suggest that these frontal systems are a major source of uncertainty in the region. Cooler ABI SST values were especially observed during the winter months, when the oceanic frontal systems have an equatorward shift (see Figure 1). Besides the challenges of matching SST measurements and products obtained at different spatial resolutions in these oceanic frontal zones, another important source of uncertainty in the region during the winter months is the frequent passage of cold atmospheric fronts, which may also lead to subpixel cloud contamination and cooler ABI SST retrievals. Positive ABI SST biases at the higher latitudes, however, remain to be further investigated.

6. Conclusions and Remarks

The present work analyzed the uncertainties of the OSI SAF SST product of the ABI sensor on board the NOAA's next generation geostationary satellite GOES-16, over the Tropical and Southwestern Atlantic Ocean. Comparisons with in situ MDBs revealed a mean bias (<0.1 °C) and error (RMSE, ~0.5 °C) within the GHRSST standards. Some uncertainties were attributed to thermal stratification, when all daytime conditions were used, and to regional/seasonal challenging conditions specific to each MDB. Some differences were also partly attributed to the uncertainties of the in situ MDBs, especially for the PNBoia moored buoys near the Brazilian coast, which are known to face challenges regarding the maintenance and calibrations of the sensors. Coastal in situ SST data are also more affected by thermal fronts (e.g., at upwelling cells) and land adjacency effects, posing significant challenges for these comparisons, which showed the highest differences. The comparisons for the drifting buoys of the PNBoia program in the Southwestern Atlantic showed low-moderate error statistics, and the uncertainties were likely associated with high SST gradients at the oceanic frontal zones and cloud contamination effects. Comparisons of the ABI SSTsat with the PIRATA moored buoys at the Tropical Atlantic showed the best results, consistent with this high quality, long-term program. Higher biases were related to cloud contamination effects and water vapor absorption, especially during the cloudiest season, with the ITCZ southward displacement.

The regional and seasonal biases of the ABI SSTsat were also indicated by a comparison with the L4 SST analysis product, reinforcing the previous analysis and highlighting some other sources of uncertainty. In the Tropical Atlantic, the highest biases were obtained at the northernmost eastern sector, and were attributed to unmasked aeolian dusts from the Sahara Desert. The second region with highest biases (up to 2 °C) were observed in the Southwestern Atlantic at the oceanic frontal zones of the BMC and STF. The middle portion of the South Atlantic basin had generally low biases (<0.1 °C) throughout most seasons, and seemed to have some higher uncertainties associated with the SACZ, likely due to cloud contamination effects.

The South Atlantic is known to be an unsampled region, with a few exceptions in the Tropical zone. The present work revealed how the "new" ABI GOES-16 SST product performs reasonably well in the study region, being suitable for operational use. Seasonal/regional biases that were pointed out are consistent with other works and highlight the need for further improvements in SST satellite retrievals, especially for the monitoring and analysis of mesoscale processes in highly dynamic frontal zones. The ABI SST product can provide high spatial-temporal information which can be broadly applied. The diurnal cycle is, for instance, a unique process measured by this product and may contribute to our understanding of the heat flux in the boundary layer, among other applications. The ABI sensor has also high spectral information collected on 16 channels, which should be further explored to improve cloud masking algorithms, processing chains, and the SST retrieval algorithm. These are some recommendations for future studies exploring the new capabilities of the ABI GOES-16 for SST satellite retrievals.

Author Contributions: Conceptualization, M.H.A., N.R. and J.A.A.; Data curation, M.H.A., N.R.; Formal analysis, M.H.A., N.R.; Investigation, M.H.A., N.R. and J.A.A.; Methodology, M.H.A., N.R. and J.A.A.; Software, M.H.A.; Supervision, N.R. and J.A.A.; Validation, M.H.A.; Visualization, M.H.A. and N.R.; Writing—original draft, M.H.A.; Writing—review & editing, N.R. and J.A.A. All authors have read and agreed to the published version of the manuscript.

Funding: This study was funded in part by the *Coordenação de Aperfeiçoamento de Pessoal de Nível Superior-Brasil* (CAPES)-Finance Code 001, with a scholarship for M. H. Azevedo.

Data Availability Statement: Publicly available datasets were analyzed in this study. The in situ data can be found here: http://www.goosbrasil.org/ and the satellite data here: https://podaac.jpl.nasa.gov/ or here: https://www.eumetsat.int/eumetsat-data-centre.

Acknowledgments: The authors acknowledge the contributions of the anonymous reviewers.

Conflicts of Interest: The authors declare no conflict of interest.

References

1. Shutler, J.D.; Quartly, G.; Donlon, C.J.; Sathyendranath, S.; Platt, T.; Chapron, B.; Johannessen, J.A.; Girard-Ardhuin, F.; Nightingale, P.D.; Woolf, D.K.; et al. Progress in satellite remote sensing for studying physical processes at the ocean surface and its borders with the atmosphere and sea ice. *Prog. Phys. Geogr. Earth Environ.* **2016**, *40*, 215–246.
2. Merchant, C.J.; Embury, O.; Bulgin, C.E.; Block, T.; Corlett, G.K.; Fiedler, E.; Good, S.A.; Mittaz, J.; Rayner, N.A.; Berry, D.; et al. Satellite-based time-series of sea-surface temperature since 1981 for climate applications. *Sci. Data* **2019**, *6*, 223.
3. Lazarus, S.M.; Calvert, C.G.; Splitt, M.; Santos, P.; Sharp, D.W.; Blottman, P.F.; Spratt, S.M. Real-time, High-resolution, space-time analysis of sea surface temperatures from multiple platforms. *Mon. Weather Rev.* **2007**, *135*, 3158–3173.
4. Le Traon, P.-Y.; Antoine, D.; Bentamy, A.; Bonekamp, H.; Breivik, L.A.; Chapron, B.; Corlett, G.; Dibarboure, G.; Digiacomo, P.; Donlon, C.; et al. Use of satellite observations for operational oceanography: Recent achievements and future prospects. *J. Oper. Oceanogr.* **2015**, *8*, S12–S27.
5. Rodgers, C.D. Retrieval of atmospheric temperature and composition from remote measurements of thermal radiation. *Rev. Geophys.* **1976**, *14*, 609.
6. Liang, X.-M.; Ignatov, A.; Kihai, Y. Implementation of the Community Radiative Transfer Model in Advanced Clear-Sky Processor for Oceans and validation against nighttime AVHRR radiances. *J. Geophys. Res.* **2009**, *114*, 06112.
7. Walton, C.C.; Pichel, W.G.; Sapper, J.F.; May, D.A. The development and operational application of nonlinear algorithms for the measurement of sea surface temperatures with the NOAA polar-orbiting environmental satellites. *J. Geophys. Res. Ocean.* **1998**, *103*, 27999–28012.
8. McClain, E.P.; Pichel, W.G.; Walton, C.C. Comparative performance of AVHRR-based multichannel sea surface temperatures. *J. Geophys. Res.* **1985**, *90*, 11587.
9. Kilpatrick, K.A.; Podestá, G.P.; Evans, R. Overview of the NOAA/NASA advanced very high resolution radiometer Pathfinder algorithm for sea surface temperature and associated matchup database. *J. Geophys. Res. Ocean.* **2001**, *106*, 9179–9197.
10. Sunder, S.; Ramsankaran, R.; Ramakrishnan, B. Machine learning techniques for regional scale estimation of high-resolution cloud-free daily sea surface temperatures from MODIS data. *ISPRS J. Photogramm. Remote Sens.* **2020**, *166*, 228–240.
11. GHRSST Science Team. *The Recommended GHRSST Data Specification (GDS) 2.0, Document Revision 4*; GHRSST Project Office: Reading, UK, 2010; p. 123.
12. Petrenko, B.; Ignatov, A.; Kihai, Y.; Pennybacker, M. Optimization of sensitivity of GOES-16 ABI sea surface temperature by matching satellite observations with L4 analysis. *Remote Sens.* **2019**, *11*, 206. [CrossRef]

13. Merchant, C.J.; Embury, O.; le Borgne, P.; Bellec, B. Saharan dust in nighttime thermal imagery: Detection and reduction of related biases in retrieved sea surface temperature. *Remote Sens. Environ.* **2006**, *104*, 15–30. [CrossRef]
14. Donlon, C.; Robinson, I.; Casey, K.S.; Vazquez-Cuervo, J.; Armstrong, E.; Arino, O.; Gentemann, C.; May, D.; LeBorgne, P.; Piollé, J.; et al. Global Ocean Data Assimilation Experiment (GODAE) High Resolution Sea Surface Temperature Pilot Project (GHRSST-PP). *Bull. Am. Meteorol. Soc.* **2007**, *88*, 8. [CrossRef]
15. A (NOAA/NESDIS/STAR) Ignatov. *GOES-R Advanced Baseline Imager (ABI) Algorithm Theoretical Basis Document for Sea Surface Temperature*; NOAA/NESDIS/STAR: College Park, MD, USA, 2010.
16. OSI SAF. *Geostationary Sea Surface Temperature Product User Manual v1.9*. SAF/OSI/CDOP3/MF/TEC/MA/181. 2018. Available online: http://www.osi-saf.org (accessed on 4 January 2021).
17. Pezzi, L.P.; Souza, R.B.; Dourado, M.S.; Garcia, C.A.E.; Mata, M.M.; Silva-Dias, M.A.F. Ocean-atmosphere in situ observations at the Brazil-Malvinas Confluence region. *Geophys. Res. Lett.* **2005**, *32*, 1–4. [CrossRef]
18. Oliveira, R.R.; Pezzi, L.P.; Souza, R.B.; Santini, M.F.; Cunha, L.C.; Pacheco, F.S. First measurements of the ocean-atmosphere CO2 fluxes at the Cabo Frio upwelling system region, Southwestern Atlantic Ocean. *Cont. Shelf Res.* **2019**, *181*, 135–142. [CrossRef]
19. Foltz, G.R.; Brandt, P.; Richter, I.; Rodríguez-Fonseca, B.; Hernandez, F.; Dengler, M.; Rodrigues, R.R.; Schmidt, J.O.; Yu, L.; Lefevre, N.; et al. The tropical atlantic observing system. *Front. Mar. Sci.* **2019**, *6*, 1–36.
20. Marinha do Brasil. *Programa Nacional De Boias—Pnboia-Plano Nacional De Trabalho*; Marinha do Brasil: Brasilia, Brazil, 2017.
21. Kodama, Y. Large-scale common features of subtropical precipitation zones (the Baiu Frontal Zone, the SPCZ, and the SACZ) Part I: Characteristics of subtropical frontal zones. *J. Meteorol. Soc. Jpn.* **1992**, *70*, 813–836. [CrossRef]
22. Schneider, T.; Bischoff, T.; Haug, G.H. Migrations and dynamics of the intertropical convergence zone. *Nature* **2014**, *513*, 45–53. [CrossRef]
23. Nielsen, D.M.; Belém, A.L.; Marton, E.; Cataldi, M. Dynamics-based regression models for the South Atlantic Convergence Zone. *Clim. Dyn.* **2019**, *52*, 5527–5553. [CrossRef]
24. Morel, X.; Lucas, M.A.; Santos, F.D. A Lagrangian study of the Brazil-Malvinas confluence: Lagrangian coherent structures and several lyapunov exponents. *J. Oper. Oceanogr.* **2014**, *7*, 13–23. [CrossRef]
25. Matano, R.P.; Palma, E.D.; Piola, A.R. The influence of the Brazil and Malvinas Currents on the Southwestern Atlantic Shelf circulation. *Ocean Sci.* **2010**, *6*, 983–995. [CrossRef]
26. Peterson, R.G.; Stramma, L. Upper-level circulation in the South Atlantic Ocean. *Prog. Oceanogr.* **1991**, *26*, 1–73. [CrossRef]
27. Donlon, C.J.; Minnett, P.J.; Gentemann, C.; Nightingale, T.J.; Barton, I.J.; Ward, B.; Murray, M.J. Toward improved validation of satellite sea surface skin temperature measurements for climate research. *J. Clim.* **2002**, *15*, 353–369. [CrossRef]
28. Derrien, M.; le Gléau, H. MSG/SEVIRI cloud mask and type from SAFNWC. *Int. J. Remote Sens.* **2005**, *26*, 4707–4732. [CrossRef]
29. Merchant, C.J.; le Borgne, P.; Roquet, H.; Marsouin, A. Sea surface temperature from a geostationary satellite by optimal estimation. *Remote Sens. Environ.* **2009**, *113*, 445–457. [CrossRef]
30. le Borgne, P.; Roquet, H.; Merchant, C.J. Estimation of Sea Surface Temperature from the Spinning Enhanced Visible and Infrared Imager, improved using numerical weather prediction. *Remote Sens. Environ.* **2011**, *115*, 55–65. [CrossRef]
31. François, C.; Brisson, A.; le Borgne, P.; Marsouin, A. Definition of a radiosounding database for sea surface brightness temperature simulations. *Remote Sens. Environ.* **2002**, *81*, 309–326. [CrossRef]
32. Donlon, C.J.; Martin, M.; Stark, J.; Roberts-Jones, J.; Fiedler, E.; Wimmer, W. The Operational Sea Surface Temperature and Sea Ice Analysis (OSTIA) system. *Remote Sens. Environ.* **2012**, *116*, 140–158. [CrossRef]
33. OSI SAF. *Global Sea Ice Concentration Reprocessing Product User Manual v 2.0*; OSI SAF, 2015; p. 32. Available online: http://www.osi-saf.org (accessed on 4 January 2021).
34. Lorenc, A.C.; Bell, R.S.; Macpherson, B. The Meteorological Office analysis correction data assimilation scheme. *Q. J. R. Meteorol. Soc.* **1991**, *117*, 59–89. [CrossRef]
35. Martin, M.J.; Hines, A.; Bell, M.J. Data assimilation in the FOAM operational short-range ocean forecasting system: A description of the scheme and its impact. *Q. J. R. Meteorol. Soc.* **2007**, *133*, 981–995. [CrossRef]
36. Picart, S.S.; Marsouin, A. Geostationary Satellite Sea Surface Temperature Scientific Validation Report Meteosat SST: OSI-206-a GOES-East SST: OSI-207-a Meteosat Indian Ocean SST: OSI-IO-SST v1.0. 2018. Available online: http://www.osi-saf.org (accessed on 4 January 2021).
37. Kurihara, Y.; Murakami, H.; Kachi, M. Sea surface temperature from the new Japanese geostationary meteorological Himawari-8 satellite. *Geophys. Res. Lett.* **2016**, *43*, 1234–1240. [CrossRef]
38. Woo, H.J.; Park, K.A.; Li, X.; Lee, E.Y. Sea surface temperature retrieval from the first Korean geostationary satellite COMS data: Validation and error assessment. *Remote Sens.* **2018**, *10*, 1916. [CrossRef]
39. Marquis, J.W.; Bogdanoff, A.; Campbell, J.R.; Cummings, J.A.; Westphal, D.L.; Smith, N.J.; Zhang, J. Estimating infrared radiometric satellite sea surface temperature retrieval cold biases in the tropics due to unscreened optically thin cirrus clouds. *J. Atmos. Ocean. Technol.* **2017**, *34*, 355–373. [CrossRef]
40. Stark, J.D.; Donlon, C.; O'Carroll, A.; Corlett, G. Determination of AATSR biases using the OSTIA SST analysis system and a matchup database. *J. Atmos. Ocean. Technol.* **2008**, *25*, 1208–1217. [CrossRef]
41. Möller, O.O.; Piola, A.R.; Freitas, A.C.; Campos, E.J.D. The effects of river discharge and seasonal winds on the shelf off southeastern South America. *Cont. Shelf Res.* **2008**, *28*, 1607–1624. [CrossRef]

42. Brewin, R.J.W.; Smale, D.A.; Moore, P.J.; Nencioli, F.; Miller, P.I.; Taylor, B.H.; Smyth, T.J.; Fishwick, J.; Yang, M. Evaluating Operational AVHRR Sea Surface Temperature Data at the Coastline Using Benthic Temperature Loggers. *Remote Sens.* **2018**, *10*, 925. [CrossRef]
43. Yang, M.; Guan, L.; Beggs, H.; Morgan, N.; Kurihara, Y.; Kachi, M. Comparison of Himawari-8 AHI SST with shipboard skin SST measurements in the Australian region. *Remote Sens.* **2020**, *12*, 1237. [CrossRef]